Morphology Determination of Functional Poly[2-methoxy-5-(3,7-dimethyloctyloxy)-1,4-phenylenevinylene]/Poly[oxa-1,4-phenylene-1,2-(1-cyanovinylene)-2-methoxy,5-(3,7-dimethyloctyloxy)-1,4-phenylene-1,2-(2-cyanovinylene)-1,4-phenylene] Blends as Used for All-Polymer Solar Cells

Joachim Loos,[1,2] Xiaoniu Yang,[2,3,] Marc M. Koetse,[2,4] Jörgen Sweelssen,[4] Herman F. M. Schoo,[2,4] Sjoerd C. Veenstra,[5] Werner Grogger,[6] Gerald Kothleitner,[6] Ferdinand Hofer[6]

[1]*Laboratory of Polymer Technology and Materials and Interface Chemistry, Eindhoven University of Technology, P.O. Box 513, NL-5600 MB Eindhoven, The Netherlands*
[2]*Dutch Polymer Institute, P.O. Box 902, NL-5600 AX Eindhoven, The Netherlands*
[3]*Group Polymer Physics, Eindhoven University of Technology, P.O. Box 513, NL-5600 MB Eindhoven, The Netherlands*
[4]*TNO Industrial Technology, P.O. Box 6235, 5600 HE Eindhoven, The Netherlands*
[5]*Energy Research Centre of the Netherlands, P.O. Box 1, 1755 ZG Petten, The Netherlands*
[6]*Research Institute for Electron Microscopy, Graz University of Technology, Steyrergasse 17, A-8010, Graz, Austria*

Received 16 January 2004; accepted 9 July 2004
DOI 10.1002/app.21822
Published online in Wiley InterScience (www.interscience.wiley.com).

ABSTRACT: Poly[2-methoxy-5-(3,7-dimethyloctyloxy)-1,4-phenylenevinylene] (MDMO-PPV) blended with poly[oxa-1,4-phenylene-1,2-(1-cyanovinylene)-2-methoxy,5-(3,7-dimethyloctyloxy)-1,4-phenylene-1,2-(2-cyanovinylene)-1,4-phenylene] (PCNEPV) has been used as the active layer for an all-polymer photovoltaic cell. The photovoltaic performance of devices is improved by a thermal treatment, which alters the morphology of the active layer. The morphology of the MDMO-PPV/PCNEPV blend has been studied with conventional transmission electron microscopy and energy-filtered transmission electron microscopy based on electron energy loss spectroscopy. The nitrogen of the cyano group within the PCNEPV has been be detected, and two-dimensional nitrogen distribution maps have been acquired. Nitrogen-rich domains have a size of approximately 20–50 nm and are homogeneously distributed over the entire film. © 2005 Wiley Periodicals, Inc. J Appl Polym Sci 97: 1001–1007, 2005

Key words: morphology; thin films; conducting polymers; TEM; EELS

INTRODUCTION

The characteristic structure of polymer photovoltaic (PV) cells and polymer light-emitting diodes (LEDs) consists of an approximately 100-nm thin active layer covered with a transparent front electrode and a metal back electrode.[1] Additional layers are often introduced to enhance charge transport, promote the injection or collection of charges, or to control the zone in which the generation (in solar cells) or recombination (in LEDs) of charge carriers occurs. For PV applications, successful examples for the composition of the active layer are polymer/fullerene blends,[2,3] polymer/inorganic semiconductor hybrids[4,5] and polymer/polymer blends.[6–8] One major drawback of the two first mentioned polymer PV systems is that the fullerenes (and their derivatives) as well as the conducting oxides absorb visible light poorly.[9] In contrast, polymer/polymer or so-called all-polymer solar cells have the specific advantage, as long as the combination of p- and n-type polymers is chosen well, that a broad absorption band can be achieved with a reasonable mixing ratio. A few examples of such blends are known in the literature, including a blend of a poly(phenylenevinylene) derivative (MEH-PPV) with the cyano-substituted variant (CN-PPV) of this polymer[6,7] and a blend of p- and n-type fluorine derivatives.[8] Another advantage of these all-polymer systems is that the polymers can be altered through a relatively easy method in such a way that optimum performance and processability can be attained.

The chemical composition, the applied processing conditions, which result in a specific thickness and roughness of the layers, and the interfacial integrity of the layers have been identified as important parameters for the performance of an organic PV device. However, the establishment of precise relations between these parameters and device performance is

Correspondence to: J. Loos (j.loos@tue.nl).

© 2005 Wiley Periodicals, Inc.

presently limited by the lack of methods for structural, compositional, and morphological analysis of the active layer and as-prepared devices. To control the organization of the active layer and its interfaces so as to tailor the functionality of the final device, deep insight into structure–property relations is imperative. Thus, state-of-the-art characterization techniques are required. In this context, transmission electron microscopy (TEM) is one of the most powerful tools. With conventional TEM, the imaging of structures and their surfaces and interfaces with a lateral resolution down to the subnanometer scale and the simultaneous analysis of the internal organization of these structures by means of electron diffraction and dark-field imaging are well-established techniques in (condensed) materials science.

For all-polymer solar cells, obtaining satisfying contrast between the two polymer components with TEM is a major problem, which is caused by the specific characteristics of the materials: in general, they consist mainly of carbon and hydrogen, and at least in this case, they are amorphous. However, there are possibilities of overcoming this limitation of conventional TEM. Recently, with the development of modern imaging filters, energy-filtered transmission electron microscopy (EFTEM) has emerged as a powerful tool for materials analysis.[10,11] With electrons with an energy loss characteristic of an atomic core level, quantitative two-dimensional elemental distribution maps can be obtained in a fast, parallel fashion with nanometer resolution and high chemical accuracy.[12] In addition to providing quantitative compositional data, the electron energy loss spectrum contains chemical and solid-state information encoded in the shapes of the ionization edges. As far as macromolecular nanostructures are concerned, their high sensitivity to the electron beam requires particular attention to experimental conditions to obtain the characteristic excitation spectrum before significant damage occurs. However, the ability to record efficiently spatially resolved spectroscopic information with nanometer resolution represents the prominent advantage of the EFTEM technique. Some examples of successful applications of EFTEM in the analysis of polymer systems can be found in the work of Varlot and coworkers.[13,14]

In this study, we have applied EFTEM and electron energy loss spectroscopy (EELS) for the morphology determination of a blend of poly[2-methoxy-5-(3,7-dimethyloctyloxy)-1,4-phenylenevinylene] (MDMO-PPV) and poly[oxa-1,4-phenylene-1,2-(1-cyanovinylene)-2-methoxy,5-(3,7-dimethyloctyloxy)-1,4-phenylene-1,2-(2-cyanovinylene)-1,4-phenylene] (PCNEPV), as it is used for all-polymer solar cells. The samples for the EFTEM and EELS investigations have been prepared similarly to the route used for working PV device fabrication, and so the obtained morphology can be related to the performance of all-polymer solar cells.

EXPERIMENTAL

As a p-type material, we used MDMO-PPV synthesized by TNO Industrial Technology (Eindhoven, The Netherlands) via a sulfoxy route.[15] The n-type material was PCNEPV. More details on the preparation of the material can be found in ref. 16.

Glass substrates with patterned indium tin oxide electrodes were obtained from Philips Research (Eindhoven, The Netherlands). The substrates were carefully cleaned and treated with O_3 before use. On the substrates, an approximately 60-nm layer of PEDOT:PSS (Baytron-P, Bayer, Leverkusen, Germany) was spin-coated. The active layer was spun from a 0.4 wt % solution in chlorobenzene (Aldrich; high-performance-liquid-chromatography-grade) with a 1:1 ratio of the active materials. The concentration and spin-coating conditions were adjusted to form an active layer 30–40 nm thick. As known from other studies, PV devices based on the materials show good performance only after annealing; possible reasons are discussed elsewhere.[16,17] Thus, an additional heat treatment was performed; the samples were annealed in a nitrogen atmosphere on a hot plate at 80°C for 30 min. For the TEM investigation of the morphology, the active blend layer was removed from the substrate by selective floating on water and subsequently deposited onto a 400-mesh copper grid.

TEM measurements were conducted with a JEOL JEM-2000FX transmission electron microscope (Tokyo, Japan) operated at 80 kV and a Philips CM20 (Eindhoven, The Netherlands) operated at 200 kV; both had an LaB_6 electron gun. EFTEM and EELS were performed with a Philips CM20 TEM instrument equipped with a Gatan image filter (GIF 200); a 3-mm aperture was used for imaging, and the energy resolution was better than 1 eV in the spectroscopy mode. Comprehensive surveys on EFTEM and EELS can be found in the books of Ludwig[18] and Egerton,[19] respectively.

RESULTS AND DISCUSSION

Theoretical calculations in the maximum exciton diffusion range indicate that the ideal domain size of the donor material is on the order of tens of nanometers for the best performance of all-polymer PV devices.[20–23] Thus, besides the use of molecules having promising physical properties, the control of their organization on a local length scale via the applied processing route is essential.[24] It is known from the literature that already the solvent used may force the formation of agglomeration in solution, which results in fine and homogeneous phase separation in the case of a good solvent, whereas a less preferred or bad solvent forces a large phase separation with a broad size distribution.[25]

A similar strong dependence of the resulting morphology under the applied preparation conditions is

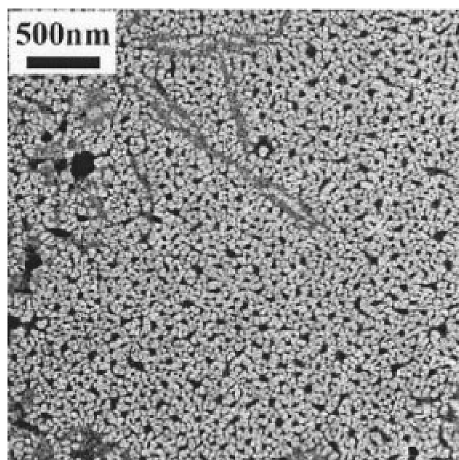

Figure 1 Bright-field TEM micrograph of the MDMO-PPV/PCNEPV blend after spin coating and before annealing.

anticipated for the MDMO-PPV/PCNEPV blend used as the active layer in an all-polymer solar cell. Figure 1 shows a TEM micrograph of the MDMO-PPV/PCNEPV blend after spin coating onto the glass substrate. With bright-field conditions, the appearance of the film is rather heterogeneous, and large regions with different contrast can be distinguished. As revealed by atomic force microscopy (AFM) investigations of the topography of the blend layer and by corresponding thickness maps with EFTEM (the acquisition and interpretation of the thickness maps are discussed later), the observed contrast in the TEM bright-field image results from thickness variations rather than from phases of different compositions. Dewetting of PCNEPV with the substrate might cause these thickness variations. A discussion of the specific dewetting and film formation characteristics of MDMO-PPV/PCNEPV blends can be found in ref. 16.

Annealing the sample changes the performance and appearance of the active layer significantly; the efficiency is doubled to 0.52%, and a homogeneous film morphology can be observed with TEM under bright-field conditions [Fig. 2(a)]. In this case, the MDMO-PPV/PCNEPV layer is removed from its substrate after annealing. Performing the annealing of the film on the TEM grid after its removal from the substrate results in a similar morphology. Imaging at a higher resolution reveals some morphological features, which can be attributed to some heterogeneity (e.g., thickness variations) of the film [Fig. 2(b)]. However, monitoring of the distinct details of the phase separation and the local organization on the nanometer scale of the functional blend is difficult with bright-field conditions. Because both components consist mainly of carbon, amplitude contrast does not exist. Phase contrast also cannot be produced, both materials have a similar electron density, and both are amorphous. Finally, in contrast to MEH-PPV/CN-PPV active blends,[6] staining with heavy elements (e.g., uranium, osmium, ruthenium, iodine, and iron) does not result in any improvement of the contrast between the two components of the blend; both are similarly sensitive to the applied staining procedures.

However, looking to the chemical structure of the two components of the blend under investigation, we find that the PCNEPV component has two nitrogen atoms in each repeat unit of its backbone. Thus, it is possible to apply EELS and EFTEM to detect the chemical compositions of the materials and to visualize their distribution within thin films.

Figure 3(a) presents a characteristic EELS spectrum of the MDMO-PPV/PCNEPV blend sample. The zero-

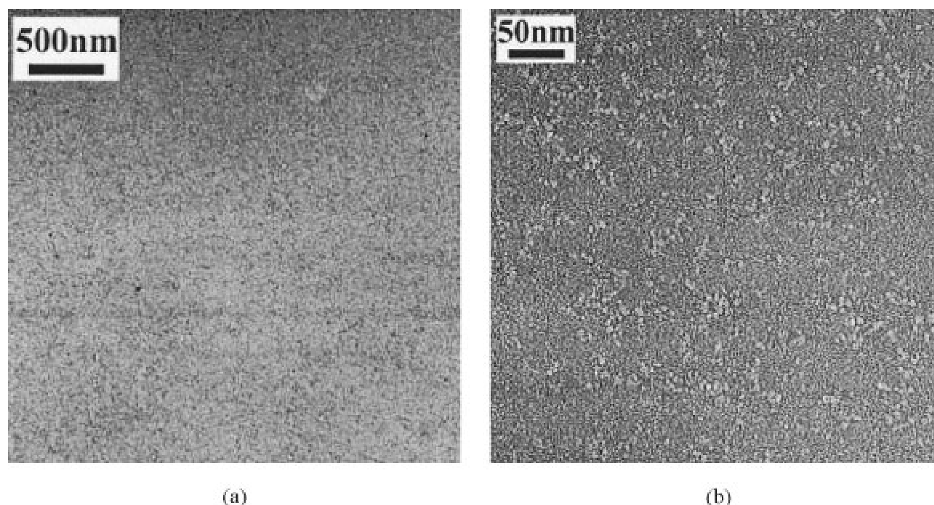

Figure 2 Bright-field TEM micrographs of the MDMO-PPV/PCNEPV blend after annealing: (a) overview and (b) higher magnification.

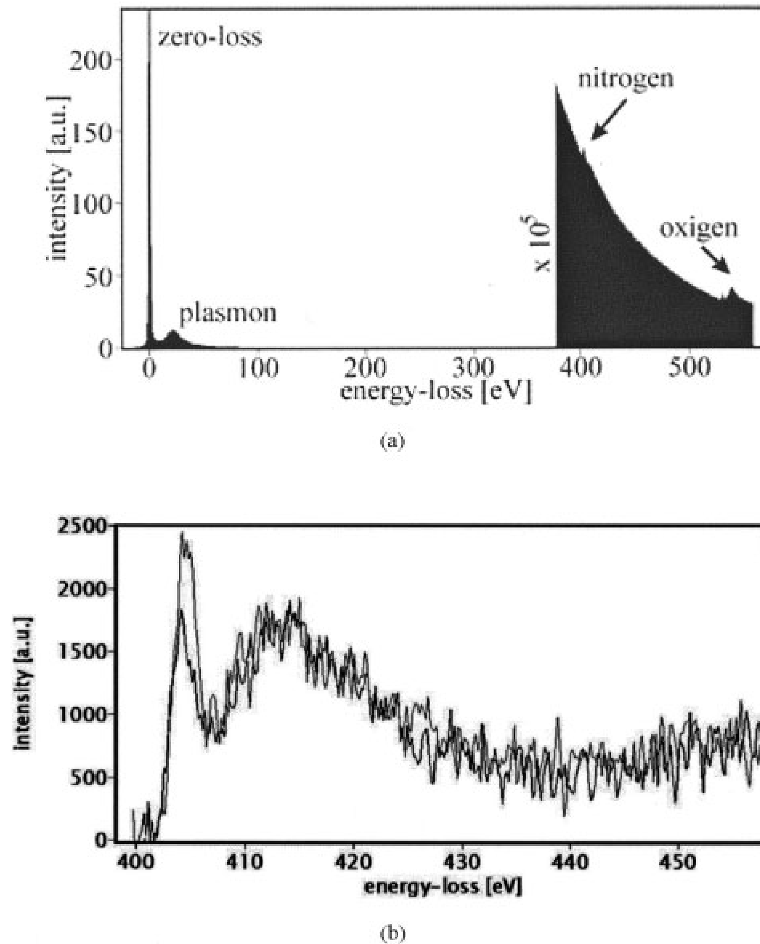

Figure 3 (a) Characteristic EELS spectrum of the MDMO-PPV/PCNEPV blend and (b) spectra acquired without any pre-exposure of the sample to the electron beam (light gray) and for a second acquisition in the same area (dark gray). The acquisition time was 30 s.

loss peak and the broad plasmon region are shown at a low energy loss. At energy losses of 401 and 532 eV, the presence of nitrogen and oxygen, respectively, can be detected. The high energy loss part of the spectrum is enlarged by a factor of 10^5. The nitrogen signal is very weak, and with exposure time, the intensity of the signal diminishes. Figure 3(b) shows the overlay of two EELS spectra acquired in 30 s without any pre-exposure of the sample to the electron beam and for a second acquisition in the same area. It is known that halogens, as well as nitrogen, fade away under the irradiation of an electron beam *in vacuo* (knock-on damage).[26] However, in this case, we were able to use the electron energy loss signal of nitrogen for the successful detection of its distribution within the sample by applying EFTEM.

Figure 4 shows a region similar to that shown in Figure 2(b) but after energy filtration with an energy slit width of 10 eV: Figure 4(a) is an unfiltered image, whereas the image of Figure 4(b) has been zero-loss-filtered. Especially in the latter case, the contrast between the phases is increased; dark gray domains 10–50 nm in size are visible. This contrast increase can be attributed to the fact that inelastic cross sections for the elements up to atomic number $(Z) = 12$ are larger than the elastic ones; hence, filtering the inelastically scattered electrons largely reduces chromatic blurring and diffuse background intensity.

In this case, the contrast is not a result of thickness variations within the film sample; this can be seen from the thickness map in Figure 5(a). From an electron energy loss spectrum and from EFTEM, the thickness from both crystalline and amorphous materials in terms of the total inelastic mean free path (λ) can be conveniently estimated. The probability of plural scattering in EELS can be described by Poisson statistics, and as a result, the ratio of the specimen thickness (t) to λ is given by ref. 27:

$$\frac{t}{\lambda} = \ln\left(\frac{I_t}{I_0}\right) \tag{1}$$

where I_t is the total integrated spectral intensity and I_0 is the zero-loss integral. If the mean free path for

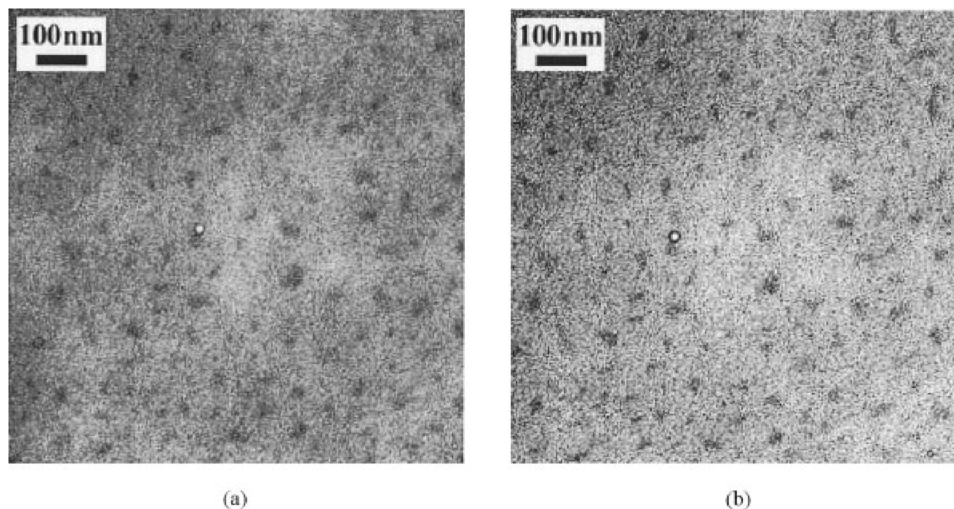

Figure 4 (a) Unfiltered and (b) zero-loss-filtered TEM images of the same region shown in Figure 2(b).

inelastically scattered electrons is identical within the whole sample (i.e., the sample is composed mainly of the same atoms), even a somewhat quantitative thickness map can be calculated. Looking in more detail at the thickness map, we can see slight variations of the contrast; however, the gray scale or intensity histogram of Figure 5(a) [Fig. 5(b)] tells us that because of its narrow distribution, the film is homogeneous in thickness. With λ = 138 nm for carbon, an applied acceleration voltage of 200 kV, and a collection angle of 7.6 mrad,[28] the film thickness is approximately 30 nm. This result is also supported by additional AFM measurements.

Figure 6 shows a bright-field TEM image and the corresponding N–K elemental distribution image of the same area. The latter visualizes the nitrogen distribution within the thin MDMO-PPV/PCNEPV film sample. In the bright-field image, some darker regions can be clearly distinguished [Fig. 6(a)]. With EFTEM, an electron spectroscopy image may be acquired at or beyond an ionization-edge absorption energy corresponding to a specific elemental species. Such a postedge image contains information regarding the spatial distribution and concentration of the chosen element, with an additional underlying background contribution corresponding to a variety of inelastic events occurring at lower energy losses. Therefore, to obtain an elemental distribution map from a core-loss image, the spectral background contribution must be taken into consideration. For the nitrogen mapping, the three-window technique has been applied;[29] that is, measurements in the pre-edge and postedge regions of the nitrogen peak have been made for the calculation of the signal's background with the power-law fit. The

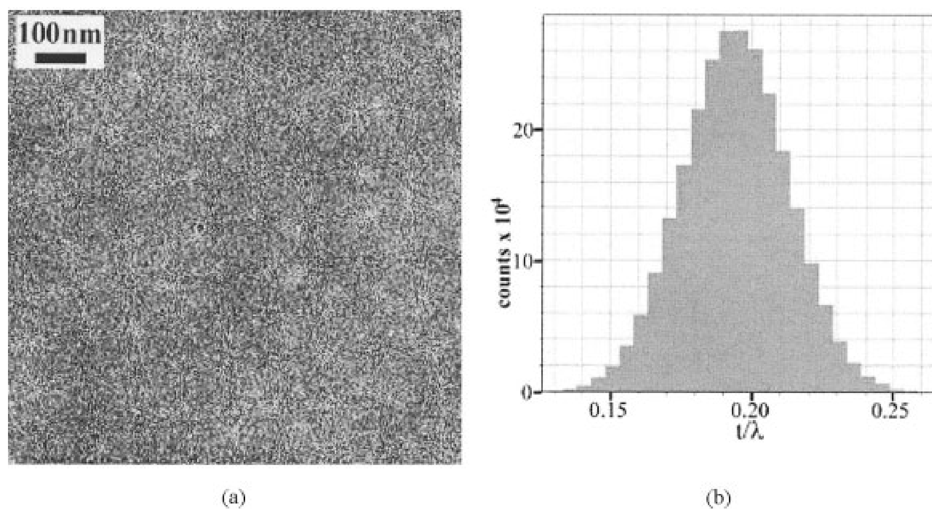

Figure 5 (a) Thickness map and (b) corresponding intensity histogram of the same region shown in Figure 4.

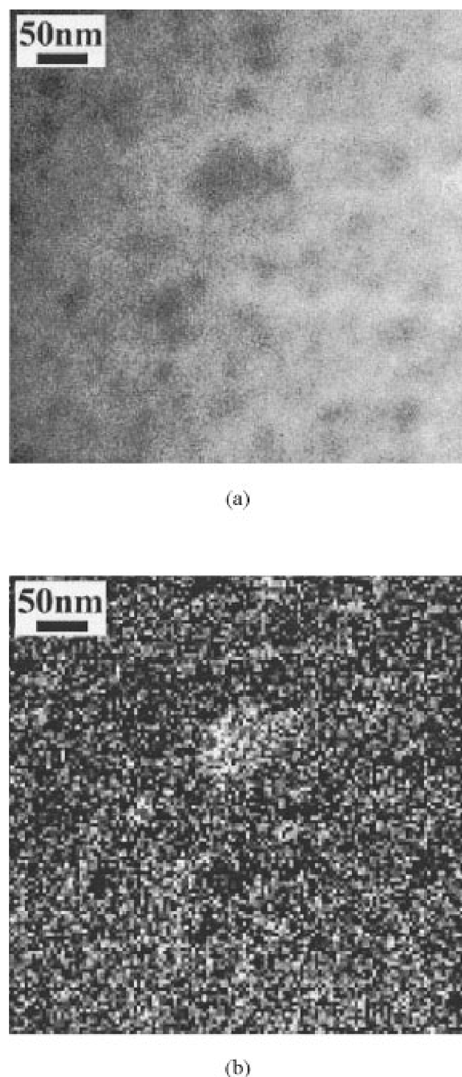

Figure 6 (a) Zero-loss-filtered TEM and (b) corresponding N–K elemental map of the same area. The latter visualizes the nitrogen distribution within the MDMO-PPV/PCNEPV film sample.

signal-to-noise ratio is rather low, but distinct regions showing higher nitrogen intensity can be identified [Fig. 6(b)]. In particular, the central bright domain, which has a size of approximately 50 nm, can be easily correlated with the central dark gray domain of the corresponding bright-field TEM image of Figure 6(a). Keeping in mind that the nitrogen concentration in PCNEPV is only approximately 5.3 wt %, we find the result of the elemental mapping to be very satisfying.

Through the combination of these results, the correlation of nitrogen-rich domains with the presence of PCNEPV phases within the MDMO-PPV matrix can be executed. However, on the basis of the overview images, it seems that the PCNEPV domains do not fill 50% of the sample, as they should in a 1:1 MDMO-PPV/PCNEPV blend. Thus, the term *nitrogen-rich* has to be interpreted in such a way that only the enrichment of nitrogen can be detected; PCNEPV molecules can still also be present in the less rich nitrogen regions of the sample. Additional model systems with, for example, various component concentrations are currently being used for a more detailed investigation of the phase separation and its relation with the applied preparation conditions, and this may improve our understanding of the phase separation and its mechanism for MDMO-PPV/PCNEPV blends as used as active layers in all-polymer PV devices.

CONCLUSIONS

The relationship of the local organization and the overall morphology with the functionality of active layers as used for all-polymer solar cells is essential for optimizing the performance of such devices. For all-polymer devices, the contrast between the components of the active layer is limited when conventional TEM is used, and this prevents detailed investigations of the phase demixing behavior on the nanometer scale.

In this study, we have presented first results related to morphology visualization in thin films of a functional MDMO-PPV/PCNEPV blend with EELS, EFTEM, and conventional TEM. The as-prepared samples had large thickness variations; however, after annealing, the samples showed enhanced efficiency and homogeneous thickness. The latter was measured with thickness maps, and an average thickness of 30 nm was calculated. With the help of EELS, the nitrogen of PCNEPV was detected, and nitrogen maps were successfully calculated. Nitrogen-rich domains approximately 20–50 nm in size were homogeneously distributed over the entire film sample. The correlation of the EFTEM results (elastic and inelastic scattered electron imaging) with conventional bright-field TEM of the same region showed that even with conventional TEM, a slight contrast between the phases was present; however, applying zero-loss filtering resulted in a more distinct differentiation of the phase distribution and size throughout the sample.

With the presented investigation route, a systematic study of the influence of the molecular architecture of PCNEPV derivatives, such as variations of the molecular weight and side-chain branching, on the performance of the introduced all-polymer PV devices is currently in progress. In addition, using EELS and EFTEM at the temperature of liquid nitrogen or liquid helium may enhance the signal-to-noise ratio significantly, and this may aid in the detection of PCNEPV even in less nitrogen-enriched regions.

The work of one of the authors (X.Y.) forms part of the research program of the Dutch Polymer Institute. The authors thank Sasha Alexeev for his supporting atomic force microscopy investigations and Martijn Wienk for discussion.

Special thanks from one of the authors (J.L.) are extended to the whole team of Forschungszentrum für Elektronenmikroskopie (Graz, Austria) for its indefatigable readiness for discussions and technical and personal support.

References

1. Friend, R. H.; Gymer, R. W.; Holmes, A. B.; Burroughes, J. H.; Marks, R. N.; Taliani, C.; Bradley, D. D. C.; Dos Santos, D. A.; Brédas, J. L.; Lögdlund, M.; Salaneck, W. R. Nature 1999, 397, 121.
2. Yu, G.; Gao, J.; Hummelen, J. C.; Wudl, F.; Heeger, A. J. Science 1995, 270, 1789.
3. Shaheen, S. E.; Brabec, C. J.; Padinger, F.; Fromherz, P.; Hummelen, J. C.; Sariciftci, N. S. Appl Phys Lett 2001, 78, 841.
4. O'Regan, B.; Grätzel, M. Nature 1991, 355, 737.
5. van Hal, P. A.; Wienk, M. M.; Kroon, J. M.; Verhees, W. J. H.; Slooff, L. H.; van Gennip, W. J. H.; Jonkheijm, P.; Janssen, R. A. J. Adv Mater 2003, 15, 118.
6. Greenham, N. C.; Moratti, S. C.; Bradley, D. D. C.; Friend, R. H.; Holmes, A. B. Nature 1993, 365, 628.
7. Yu, G.; Heeger, A. J. J Appl Phys 1995, 78, 4510.
8. Halls, J. J. M.; Arias, A. C.; MacKenzie, J. D.; Wu, W.; Inbasekaran, M.; Woo, W. P.; Friend, R. H. Adv Mater 2000, 12, 498.
9. van Hal, P. A.; Christiaans, M. P. T.; Wienk, M. M.; Kroon, J. M.; Janssen, R. A. J. J Phys Chem B 1999, 103, 4352.
10. Krivanek, O. L.; Gubbens, A. J.; Dellby, N. Microsc Microanal Microstruct 1991, 2, 315.
11. Grogger, W.; Schaffer, B.; Krishnan, K. M.; Hofer, F. Ultramicroscopy 2003, 96, 481.
12. Kravinek, O. L.; Kundmann, M. K.; Kimotot, K. J Microsc 1995, 180, 277.
13. Varlot, K.; Martin, J. M.; Quet, C.; Kihn, Y. Ultramicroscopy 1997, 68, 123.
14. Varlot, K.; Martin, J. M.; Gonbeau, D.; Quet, C. Polymer 1999, 40, 5691.
15. Lutsen, L.; Adriaensens, P.; Becker, H.; van Breemen, A. J.; Vanderzande, D.; Gelan, J. Macromolecules 1999, 32, 6517.
16. Koetse, M. M.; Sweelssen, J.; Franse, T.; Veenstra, S. C.; Kroon, J. M.; Yang, X.; Alexeev, A.; Loos, J.; Schubert, U.; Schoo, H. F. M. Proc SPIE-Int Soc Opt Eng, 2004, 5215, 119.
17. Padinger, F.; Rittberger, R. S.; Sariciftci, N. S. Adv Funct Mater 2003, 13, 85.
18. Ludwig, R. Energy-Filtering Transmission Electron Microscopy; Springer Series in Optical Sciences 71; Springer-Verlag: Berlin, 1995.
19. Egerton, R. F. Electron Energy-Loss Spectroscopy in the Electron Microscope, 2nd ed.; Plenum: New York, 1996.
20. Yoshino, K.; Hong, Y. X.; Muro, K.; Kiyomatsu, S.; Morita, S.; Zakhidov, A. A.; Noguchi, T.; Ohnishi, T. Jpn J Appl Phys Part 2 1993, 32, L357.
21. Halls, J. J. M.; Pichler, K.; Friend, R. H.; Moratti, S. C.; Holmes, A. B. Appl Phys Lett 1996, 68, 3120.
22. Haugeneder, A.; Neges, M.; Kallinger, C.; Spirkl, W.; Lemmer, U.; Feldmann, J. Phys Rev B 1999, 59, 15346.
23. Savenije, T. J.; Warman, J. M.; Goossens, A. Chem Phys Lett 1998, 287, 148.
24. Shaheen, S. E.; Brabec, C. J.; Sariciftci, N. S.; Padinger, F.; Fromherz, T.; Hummelen, J. C. Appl Phys Lett 2001, 78, 841.
25. Martens, T.; Hae, J. D.; Munters, T.; Goris, L.; Beelen, Z.; Manca, J.; D'Olieslaeger, M.; Vanderzande, D.; De Schepper, L.; Andriessen, R. Mater Res Soc Proc 2002, 725, 7.11.1.
26. Mkhoyana, K. A.; Silcox, J. Appl Phys Lett 2003, 82, 859.
27. Joy, D. C.; Egerton, R. F.; Maher, D. M. Scanning Electron Microsc 1979, 2, 817.
28. Malis, T.; Cheng, S. C.; Egerton, R. F. J Electron Microsc Tech 1988, 8, 193.
29. Jeanguillaume, C.; Trebbia, P.; Colliex, C. Ultramicroscopy 1978, 3, 237.